Reflectometer sensing of rf waves in front of the high harmonic fast wave antenna on NSTX

J. B. Wilgen, P. M. Ryan, G. R. Hanson, and D. W. Swain
Oak Ridge National Laboratory, Oak Ridge, Tennessee 37831

S. I. Bernabei, N. Greenough, S. DePasquale, C. K. Phillips, J. C. Hosea, and J. R. Wilson
Princeton Plasma Physics Laboratory, Princeton, New Jersey 08543

(Received 7 May 2006; presented on 9 May 2006; accepted 6 July 2006; published online 23 October 2006)

The ability to measure rf driven waves in the edge of the plasma can help to elucidate the role that surface waves and parametric decay instabilities (PDIs) play in rf power losses on NSTX. A microwave reflectometer has recently been modified to monitor rf plasma waves in the scrape-off layer in front of the 30 MHz high harmonic fast wave antenna array on NSTX. In rf heated plasmas, the plasma-reflected microwave signal exhibits 30 MHz sidebands, due primarily to the modulation of the cutoff layer by the electrostatic component of the heating wave. Similarly, electrostatic parametric decay waves (when present) are detected at frequencies below the heating frequency, near 28, 26, … MHz, separated from the heating frequency by harmonics of the local ion cyclotron frequency of about 2 MHz. In addition, a corresponding frequency matched set of decay waves is also detected near the ion cyclotron harmonics at 2, 4, … MHz. The rf plasma-wave sensing capability is useful for determination of the PDI power threshold as a function of antenna array phasing (including toroidal wavelength), outer gap spacing, and various plasma parameters such as the magnetic field and the plasma current. © *2006 American Institute of Physics.*
[DOI: 10.1063/1.2336441]

INTRODUCTION

High harmonic fast wave (HHFW) heating has been relatively successful on NSTX. Efficient electron heating and both co- and countercurrent drive have been demonstrated,[1] with up to 120 kA of driven current.[2] However, the heating efficiencies and current drive efficiencies for some cases were lower than expected, depending primarily on the phasing of the antenna. This was suggestive of rf power losses in the surface of the plasma, such as surface waves. Another possible mechanism for rf power loss in the edge plasma was hypothesized to be the parametric decay instability (PDI), which was predicted to have a relatively low power threshold in NSTX.[3] Coincidentally, Doppler broadening of both impurity and majority ion species was observed to increase in the edge of the plasma during rf heating experiments.[4] Spectrum analyzer data obtained with a floating Langmuir probe located between two straps of the HHFW antenna revealed the characteristic spectra of the expected parametric decay waves.[5] Microwave reflectometry has previously been used to measure rf driven waves in the interior of the DIII-D plasma.[6]

DESCRIPTION OF THE HHFW REFLECTOMETER

Because plasma loading of the HHFW antenna array is sensitive to details of the electron density profile in the plasma edge region, a microwave reflectometer with access through the HHFW antenna was initially installed to measure the time-dependent edge-density profile immediately in front of the antenna during rf heating experiments.[7] A single broadband *X*-mode reflectometer covering the frequency range of 6–27 GHz provides the capability for measuring the edge-density profile from below 1.0×10^{17} m^{-3} to nearly 8×10^{18} m^{-3}. The transmitting/receiving antennas are located between two of the current straps of the HHFW antenna array, on the horizontal midplane of NSTX. A pair of circular waveguide launchers is used to provide externally adjustable wave polarization to match the pitch angle of the magnetic field at the edge of the plasma, which is typically in the range of 25°–45°. Phase detection is accomplished using a broadband (6–27 GHz) I/Q demodulator. Quadrature phase data from the FM reflectometer, which utilizes a 100 μs sweep time, are recorded using a 5 MHz sampling rate.

Reconstruction of density profiles from the FM reflectometer data is automated, with more than 1000 edge profiles generated during the 210 ms data window that is available for each shot. Individual density profiles are reconstructed from each separate frequency sweep. In addition, phase-averaged density profiles are generated at 1.8 ms intervals based on weighted averages of the phase data, depending on the quality of the phase data from each sweep. From these phase-averaged profiles, contour plots showing the time evolution of the edge-density profile are generated to display the general trends in the edge profile during rf heating experiments, as shown in Fig. 1. The individual contours track the location of densities of $(0.05,0.1,0.2,\ldots,0.6)\times10^{19}$ m^{-3} as a function of time. Distances are relative to the location of

 © 2006 American Institute of Physics

Downloaded 19 Dec 2007 to 198.35.1.10. Redistribution subject to AIP license or copyright; see http://rsi.aip.org/rsi/copyright.jsp

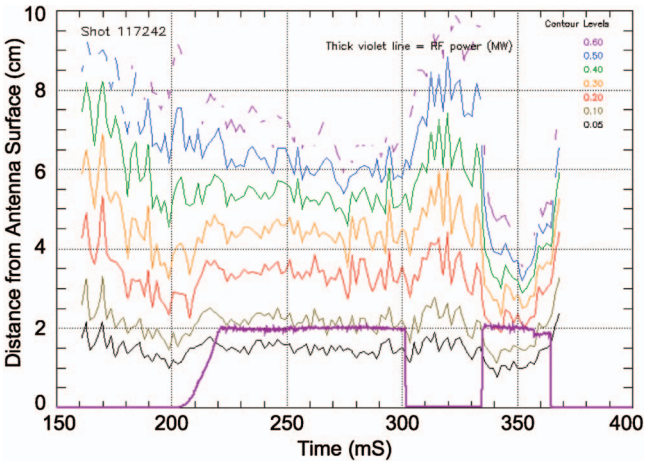

FIG. 1. (Color) Contour plot of the edge-density profile immediately in front of the HHFW antenna array. The color coded contours (black, brown, red, orange, green, blue, and violet) correspond to densities of $(0.05, 0.1, 0.2, \ldots, 0.6) \times 10^{19}$ m^{-3}, respectively. The thick violet line shows the modulation wave form of the rf power in units of megawatts.

the leading edge of the HHFW antenna. Also overplotted in Fig. 1 is the modulation wave form of the applied rf power, as shown by the thick violet line. The measured edge profiles have been utilized in calculations of plasma antenna loading using the RANT3D code,[8] which was the original motivation for installing the reflectometer.

The quadrature phase detection capability allows the reflectometer to also be utilized as a fluctuation diagnostic to characterize the frequency spectrum of density fluctuations in the edge-plasma region immediately in front of the antenna. For this mode of operation, the probing frequency of the reflectometer is set to dwell at a fixed frequency, corresponding to the cutoff density at the region of interest within the edge profile.[7] It is found that density fluctuations in the edge region are large, but have short scale length compared with the length of the current straps. Therefore, in practice, the antenna loading depends predominantly on the average edge-density profile.

rf PLASMA-WAVE MONITORING CAPABILITY

In addition to the primary function of measuring edge density profiles, the HHFW microwave reflectometer has recently been modified to monitor rf plasma waves in the scrape-off layer in front of the HHFW antenna array. rf plasma-wave-related signals are extracted from the I/Q demodulator, which has an output bandwidth of dc-500 MHz. As shown by the circuit diagram in Fig. 2, a high-pass filter is used to prevent loading/distortion of the standard FM reflectometer signals which utilize the i.f. frequency range of dc-1.4 MHz. The reflectometry derived rf signals are then amplified by about 40 dB inside the reflectometer instrument enclosure prior to transmission to the fast digitizer, taking care to minimize direct pickup of the 30 MHz heating frequency. A fast digitizer, with 100 MHz sampling rate, is used to acquire the reflectometer rf plasma wave data, as well as similar data from a floating Langmuir probe that is also located within the HHFW antenna array, recessed slightly behind the boron nitride tiles and Faraday screens. The acquired data are archived on digital versatile disks (DVD's). To provide an initial sampling of the data, fast fourier transform (FFT) spectra are generated at equally spaced intervals, typically 2 ms apart, and written to the NSTX MDSPLUS data tree. This initial sampling currently represents approximately 1% of the data.

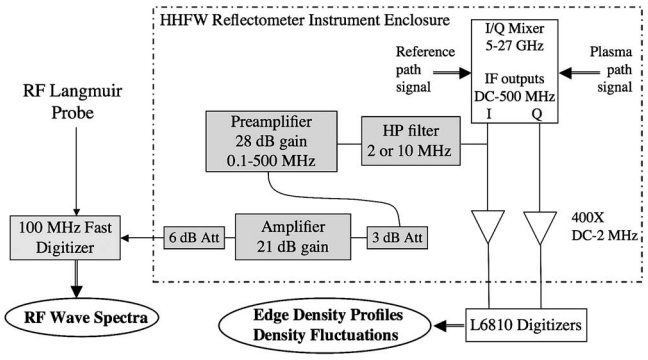

FIG. 2. Block diagram of the coupling circuit used for extraction of rf plasma wave signals from the HHFW microwave reflectometer instrument.

During rf heating experiments, the reflectometer probing beam acquires 30 MHz sidebands, primarily due to the modulation of the cutoff layer by the electrostatic component of the heating wave. Prior estimates of the magnitude of the 30 MHz density wave immediately in front of the antenna indicated that the heating wave should be readily detected by the reflectometer. In addition, it was anticipated that the daughter waves resulting from PDI activity would be readily detected based on the electrostatic nature of the predicted decay waves.

A comparison of the rf plasma-wave spectra obtained with two different phasings of the HHFW antenna array is shown in Figs. 3 and 4 in the form of contour plots of the frequency spectra as a function of time. In both cases, the heating power level is 2 MW and the last closed (outermost) flux surface is located about 4 cm in front of the antenna. For the case of current drive (−90°) phasing of the antenna array,

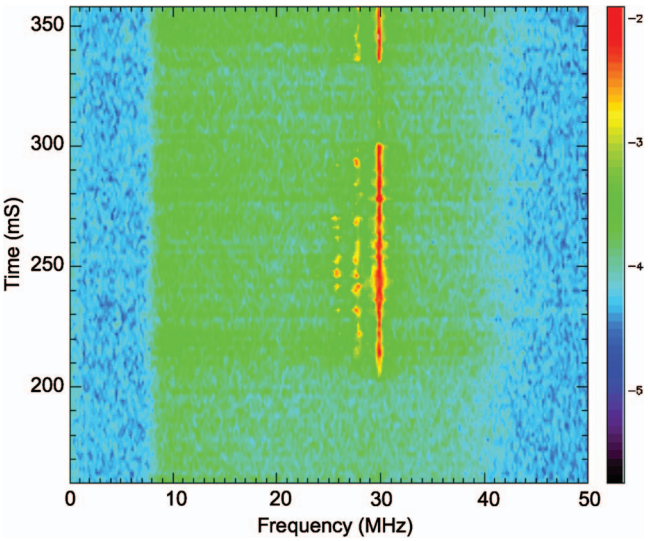

FIG. 3. (Color) Contour plot showing the time evolution of the rf plasma wave spectra for current drive phasing (−90°) of the HHFW antenna array at a rf power level of 2 MW.

Downloaded 19 Dec 2007 to 198.35.1.10. Redistribution subject to AIP license or copyright; see http://rsi.aip.org/rsi/copyright.jsp

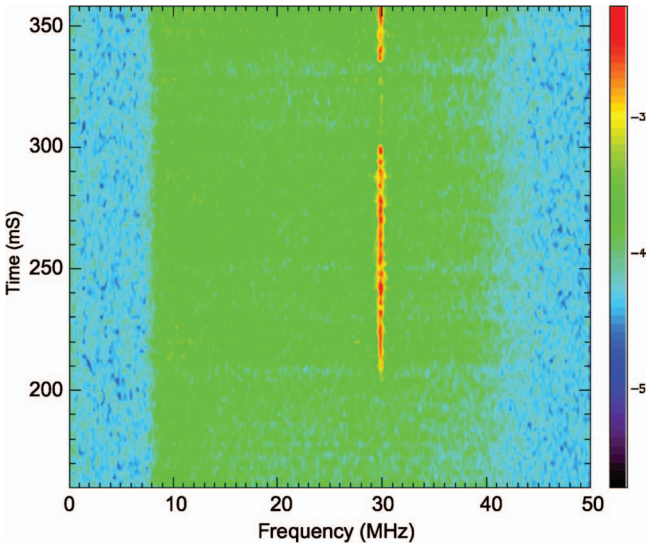

FIG. 4. (Color) Contour plot showing the time evolution of the rf plasma wave spectra for symmetric phasing (180°) of the HHFW antenna array, with 2 MW of rf heating power.

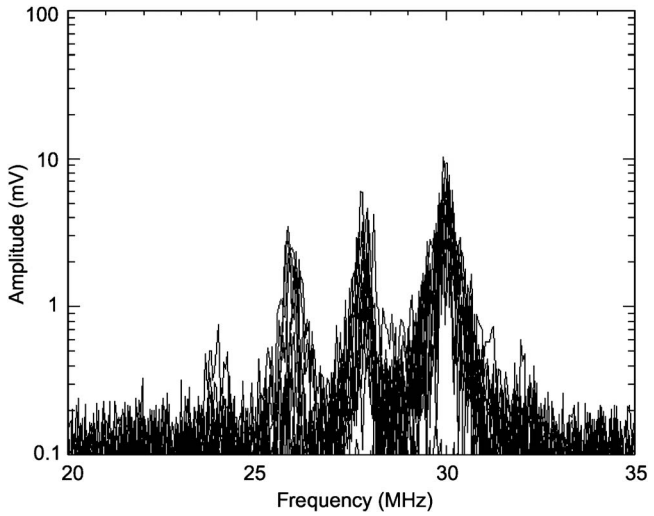

FIG. 5. Overplotting 11 individual spectra obtained during the 240–260 ms time interval from the data set shown in Fig. 3, with current drive (–90°) antenna array phasing at a rf power level of 2 MW.

shown in Fig. 3, intermittent parametric decay features are evident near 26 and 28 MHz, in addition to the 30 MHz heating frequency. By comparison, for the case of symmetric (180°) antenna array phasing, as shown in Fig. 4, only the 30 MHz heating wave is detected. It should be noted that the rf power level is varying with time, using the same power modulation wave form shown in Fig. 1. Also apparent from these two figures is the effect of the 10 MHz high-pass filter, that suppresses all signals below 8 MHz. At the upper end of the frequency range, above 40 MHz, the effect of an anti-aliasing filter is also evident. For this data, the reflectometer probing frequency was set at a fixed frequency near 17.5 GHz, corresponding to a cutoff density of about 2.5×10^{18} m^{-3}. For typical L-mode edge-profile conditions, this typically corresponds to a probing location of 3–5 cm in front of the antenna, depending on the location of the last closed flux surface and the rf power level.

In Figs. 5 and 6, a subset of the same data (from Figs. 3 and 4) is replotted, displaying a sequence of individual FFT spectra overplotted to provide a more quantitative view of the spectral features in the 20–35 MHz frequency range. In each figure, 11 spectra from the 240–260 ms time interval are shown, each of which is generated from 2048 data samples obtained during a 20 μs interval. For current drive (–90°) phasing of the antenna array, shown in Fig. 5, parametric decay frequencies are clearly evident at equally spaced frequencies near 24, 26, and 28 MHz. This frequency spacing corresponds to the local ion cyclotron frequency immediately in front of the HHFW antenna. By coincidence, the amplitudes of the parametric decay features are nearly as large as the heating-wave feature, but unlike the 30 MHz signal they are not always present. Although the heating-wave signal does show some evidence of amplitude modulation, the parametric decay features are decidedly more intermittent. By comparison, the spectra for symmetric (180°) phasing of the antenna array, shown in Fig. 6, show no evidence of PDI activity, and the amplitude of the 30 MHz signal is somewhat reduced.

It should be noted that direct 30 MHz pickup from the rf heating system was detectable but was generally small, and was readily distinguished from the heating-wave modulation of the reflectometer probing beam. During rf experiments, the HHFW reflectometer was typically switched between two modes of operation: fast-swept FM mode to obtained edge-density profiles, and fixed-frequency operation to acquire rf plasma wave data (or alternatively, density fluctuation data). In fast-swept FM mode, the heating-wave sidebands do not appear at 30 MHz, but instead are shifted by about 1 MHz, depending on the direction of the frequency sweep. This is attributable to the rapid frequency sweep rate of the FM reflectometer, 0.2 MHz/ns, and the path length difference between the two arms of the reflectometer, resulting in a time delay of 4–5 ns. Any direct pickup from the heating system is readily apparent from the remaining residual signal at 30 MHz.

Parametric decay frequencies in the 2–10 MHz range

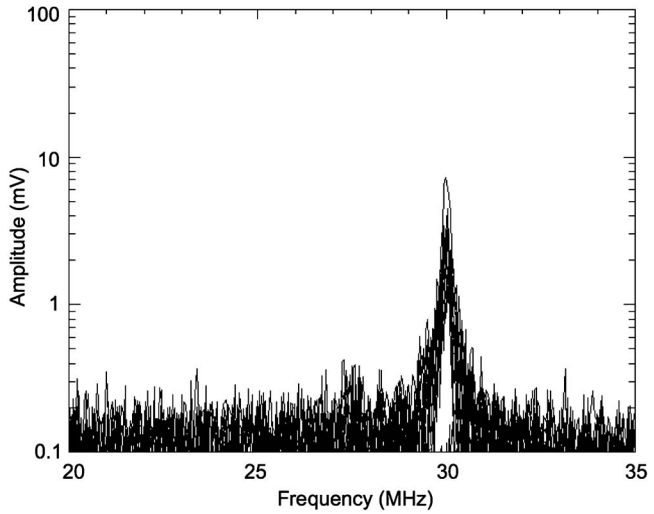

FIG. 6. Overplotting 11 consecutive spectra obtained during the 240–260 ms time interval from the data set shown previously in Fig. 4, for symmetric (180°) antenna array phasing with 2 MW of rf heating power.

Downloaded 19 Dec 2007 to 198.35.1.10. Redistribution subject to AIP license or copyright; see http://rsi.aip.org/rsi/copyright.jsp

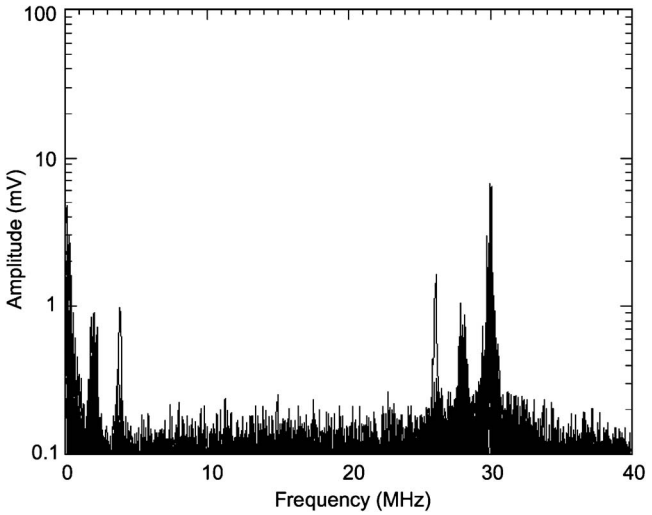

FIG. 7. Overplot of 31 spectra obtained using a 2 MHz high-pass filter, that allows the parametric decay spectra in the 2–10 MHz range to be displayed. These data were obtained with symmetric (180°) phasing to the antenna array, with 1.6 MW of rf power.

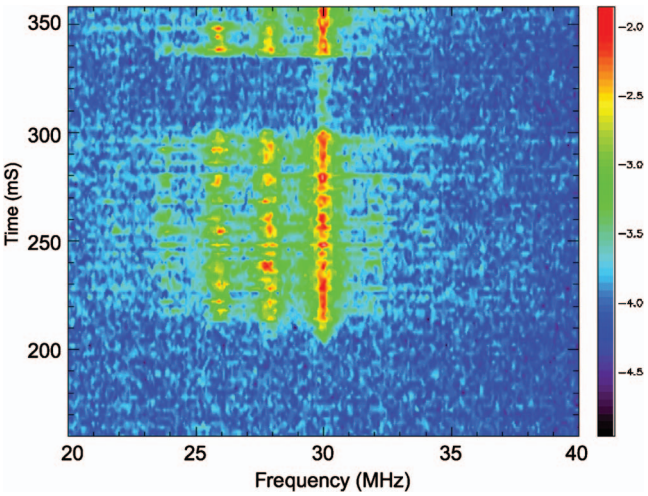

FIG. 8. (Color) During the ramp-up of the rf power starting at 200 ms, the heating wave frequency appears first at 30 MHz. Parametric decay frequencies are delayed, appearing sequentially in time. When the power is suddenly reduced by a factor of 100 times at 300 ms, the parametric decay waves disappear, but the heating wave is still readily detectable.

have also been detected, after replacing the 10 MHz high-pass filter with a 2 MHz high pass. An example of the resulting spectra is shown in Fig. 7, where 31 individual spectra are overplotted. In this instance, the parametric features near 2 and 28 MHz were present during a substantial fraction of the FFT sampling intervals, whereas the features near 4 and 26 MHz were present for only a single spectrum. These data were obtained with symmetric (180°) phasing to the antenna array. The heating power level was 1.6 MW, and the last closed (outermost) flux surface was located 2–4 cm in front of the antenna. The complete parametric decay spectra, as shown in Fig. 7, are consistent with theoretical expectations.[3]

Indications of the power threshold for PDI activity can be obtained in several ways. In Fig. 8, the heating-wave frequency was the first to appear during the ramp-up of the rf power, followed sequentially by the parametric features near 28 and 26 MHz, and occasionally at 24 MHz. The rf power was slowly ramped up starting at 200 ms, reaching full power at 220 ms. By correlating the onset time of the 28 MHz feature with the wave form of the rf heating power (shown previously in Fig. 1), the threshold for the PDI can be estimated for each heating condition (antenna array phasing, etc). Then at 300 ms, the power was rapidly reduced by 100-fold, from 2 MW to approximately 20 kW, and later returning to full power at 335 ms. Note that when the power was reduced (at 300–335 ms), the heating wave was still detected at a reduced level, whereas the PDI frequencies were absent. Varying the power setting for this modulated low-power condition provides a secondary means for investigating the power threshold. For this rf heating condition, current drive (−90°) array phasing with an 8 cm outer gap, the PDI power threshold was evidently greater than the estimated 20 kW low-power state.

ACKNOWLEDGMENTS

This work was supported at Oak Ridge National Laboratory, managed by UT-Battelle, LLC, for the U.S. Department of Energy under Contract No. DE-AC05-00OR22725, and at the Princeton Plasma Physics Laboratory under DOE Contract No. DE-AC02-76CHO3073.

[1] J. C. Hosea *et al.*, AIP Conf. Proc. **787**, 82 (2005).
[2] P. M. Ryan *et al.*, AIP Conf. Proc. **694**, 209 (2003).
[3] J. R. Wilson *et al.*, AIP Conf. Proc. **787**, 66 (2005).
[4] T. M. Biewer, R. E. Bell, S. J. Diem, C. K. Phillips, J. R. Wilson, and P. M. Ryan, Phys. Plasmas **12**, 056108 (2005).
[5] S. Diem, T. Biewer, B. LeBlanc, J. Hosea, M. Ono, C. Phillips, and J. Wilson, Bull. Am. Phys. Soc. **50**, 330 (2005).
[6] J. H. Lee, E. J. Doyle, N. C. Luhmann, Jr., W. A. Peebles, C. C. Petty, R. I. Pinsker, and T. L. Rhodes, Rev. Sci. Instrum. **68**, 462 (1997).
[7] J. B. Wilgen, G. R. Hanson, T. S. Hanson, T. S. Bigelow, D. W. Swain, P. M. Ryan, M. D. Carter, and J. R. Wilson, Bull. Am. Phys. Soc. **46**, 259 (2001).
[8] D. W. Swain, M. D. Carter, J. R. Wilson, P. M. Ryan, J. B. Wilgen, J. Hosea, and A. Rosenburg, Fusion Sci. Technol. **43**, 503 (2003).

Downloaded 19 Dec 2007 to 198.35.1.10. Redistribution subject to AIP license or copyright; see http://rsi.aip.org/rsi/copyright.jsp